Effect of the Quasi-Biennial Oscillation on Carbon Monoxide in the Stratosphere

Yuk L. Yung[1,2] (iD), **Junyang Long**[3], **Jonathan H. Jiang**[2] (iD), **Siteng Fan**[1] (iD), **Xun Jiang**[4] (iD), and **Run-Lie Shia**[1] (iD)

[1]Division of Geological and Planetary Sciences, California Institute of Technology, Pasadena, CA, USA, [2]Jet Propulsion Laboratory, California Institute of Technology, Pasadena, CA, USA, [3]School of Science and Engineering, The Chinese University of Hong Kong, Shenzhen, China, [4]Department of Earth and Atmospheric Sciences, University of Houston, Houston, TX, USA

Abstract The interannual variability of tropical carbon monoxide from the Microwave Limb Sounder over 2004–2018 period is dominated by the quasi-biennial oscillation (QBO). We simulate the carbon monoxide variability over this period using the 2-D Caltech/JPL chemistry-transport model. The chemistry-transport model includes the photochemical sources and sinks and transport driven by a stream function and eddy diffusivity derived from the assimilated winds of National Centers for Environmental Prediction Reanalysis 2. The results show good agreement between model and Microwave Limb Sounder observations. We also investigate the anomalous period 2015–2016, when the QBO winds deviated significantly from their climatological values. The model simulations could capture the QBO features in agreement with observations for the anomalous period.

1. Introduction

Carbon monoxide (CO) in the middle atmosphere is produced primarily by CO_2 photolysis in the mesosphere, with minor sources from the oxidation of CH_4 (Allen et al., 1999) and upward transport of CO from surface pollutions (Jiang et al., 2007; Schoeberl et al., 2006). The major sink for CO is the reaction with the hydroxyl radical (OH) derived from the photolysis of H_2O and the reaction between H_2O and and $O(^1D)$, an excited oxygen atom produced by the photolysis of O_3 (Allen et al., 1981). The photochemistry and transport of CO were first studied using the 1-D Caltech/JPL chemistry-transport model by Allen et al. (1981), hereafter Allen81. Microwave measurements of CO were used to deduce the existence of a stagnant region in atmospheric transport around 100 km (see Figure 2 of Allen81 for details), a result that was independently obtained by Lindzen (1981).

CO is an ideal tracer for middle atmosphere dynamics and transport for at least three reasons. (1) Its chemistry is simple, as summarized above (see Figure 6 of Allen81 for details). (2) Its chemical lifetime and its transport time scale are comparable in the middle atmosphere. They are both equal to about 1 month near 60 km (see Figure 1 of Allen81 for details), making CO sensitive to both chemistry and transport. (3) CO has strong transitions in the near infrared and microwave and can be readily measured by remote sensing techniques. Since the work of Allen81, a number of papers have been written to further our understanding of CO in the middle atmosphere using observations and modeling (Allen et al., 2000; Garcia et al., 2007; Gunson et al., 1990; Lee et al., 2011, 2013, 2018; Minschwaner et al., 2010; Ruzmaikin et al., 2014; Solomon et al., 1985).

Ruzmaikin et al. (2014) presented a 2-D pattern of solar cycle variation of CO. Lee et al. (2018) pointed out that the model simulations underestimated the mean CO amount and solar cycle variations of CO, by a factor of 3, compared to those obtained from Microwave Limb Sounder (MLS) observations. Kane (2005) and Sitnov (2008) studied the quasi-biennial oscillation (QBO) in tropospheric CO mixing ratio and column CO, respectively. QBO is defined as a quasi-biennial oscillation in the zonal wind in the stratosphere (e.g., Baldwin et al., 2001). As suggested by Plumb and Bell (1982), the meridional circulation is different during different phases of QBO. During the westerly (easterly) phase of the QBO, there is anomalous descending (rising) motion in the tropics (Plumb & Bell, 1982), which can modulate CO concentration. Using satellite column CO, Sitnov (2008) found that the column CO is greater during the westerly phase of QBO than the easterly. However, no quantitative comparison with modeling has been reported.
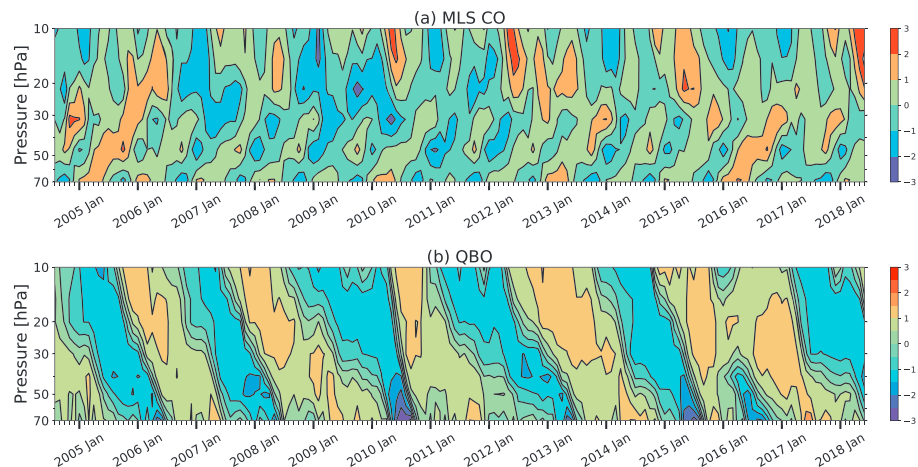
Figure 1. (a) Normalized Microwave Limb Sounder (MLS) data for CO. (b) Quasi-biennial oscillation (QBO) wind over Singapore.

The primary goal of this paper is an examination of the QBO signal in the stratosphere and a comparison of the observations to model simulations. In section 2, the data and model are presented. Section 3 shows the model results, followed by conclusions in section 4. Additional results are summarized in the supporting information.

2. Data and Model

This work is primarily motivated by the MLS measurements of CO over more than a decade (2004–2018). The Aura satellite on which the MLS instrument is aboard was launched on 15 July 2004. Aura has a Sun-synchronous orbit at an altitude of 705 km, with equatorial crossing times at 1:45 a.m. and 1:45 p.m. local solar time, and a 16-day repeat cycle (Waters et al., 2006). MLS makes measurements of CO at 240 GHz, with a vertical resolution of ~4 km and horizontal resolutions of ~6 and 400 km cross and along track in the tropical region, respectively (Livesey et al., 2008, 2015). In this study, MLS V4.2 Level 2 CO data are used. Quality control has been applied using recommended procedures (Livesey et al., 2015). The estimated single-measurement precision is ~19 ppbv for CO (Huang et al., 2016; Livesey et al., 2015).

In order to understand the mechanism that produces the QBO signal in the MLS data, we study what a model predicts and compare the results with the data. The 2-D Caltech/JPL chemistry-transport model (CTM), called KINETICS (Jiang et al., 2004; Morgan et al., 2004; Shia et al., 1989), is used in this paper to simulate CO concentration. It has 40 vertical layers covering from the surface to 0.01 hPa. There are 18 latitude boxes spaced equally from the South Pole to the North Pole. Stream functions and horizontal eddy diffusivities, K_{yy}, are derived from the National Centers for Environmental Prediction 2 (NCEP2) Reanalysis data from 1979 to 2018 (Jiang et al., 2004; Kistler et al., 2001). Since the NCEP2 Reanalysis data do not have data for pressure <3 hPa, we use the climatologically stream function derived from Fleming et al. (2002) when pressure is less than 3 hPa. The merged stream function can capture the correct age of air in the stratosphere (Morgan et al., 2004). Since the QBO signal dominates in the stratosphere, the adopting of climatology stream function above 3 hPa will not have a large influence on the CO simulation in the stratosphere. The vertical eddy diffusivities, K_{zz}, are taken from Summers et al. (1997). In our previous study (Jiang et al., 2004), we have used the stream function calculated from NCEP2 and ECMWF. We found that the stream function derived from NCEP2 Reanalysis produced the best result in simulating ozone, which might be related to different data assimilation schemes used in these reanalyses (Jiang et al., 2004). All gas-phase chemistry recommended by NASA for stratospheric modeling is included in the 2-D Caltech/JPL CTM (DeMore et al., 1997). The lower boundary of the model is at the surface, where the CO mixing ratio is set to be 64 ppbv for clean air. The upper boundary of the model is at 0.01 hPa, where we estimate a downward flux of 2.5×10^9 molecules·cm^{-2}·s^{-1} derived from the region above the upper boundary.
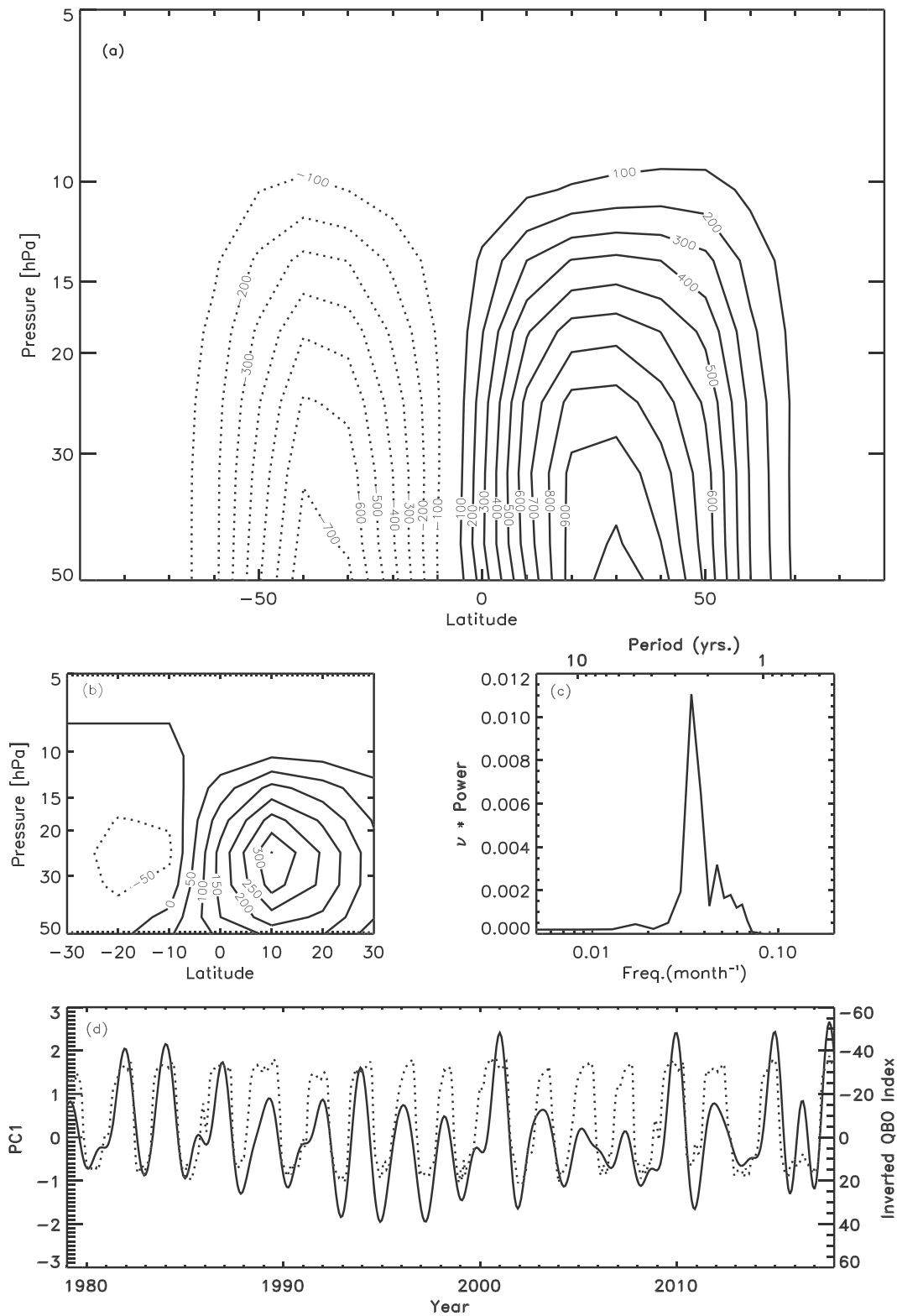
Figure 2. (a) Climatology of National Centers for Environmental Prediction 2 (NCEP2) stream function from January 1979 to August 2018. Units are square meters per second. Solid contours represent clockwise motions. Dotted lines represent counterclockwise motions. (b) Spatial pattern of the first leading empirical orthogonal function (EOF) of NCEP2 stream function. Units are square meters per second. (c) Power spectrum of the first principal component time series. (d) Principal component 1 time series (solid line) for the first EOF of NCEP2 stream function and inverted 20-hPa quasi-biennial oscillation index (dotted line).

Figure 3. Normalized model CO mixing ratio.

3. Results

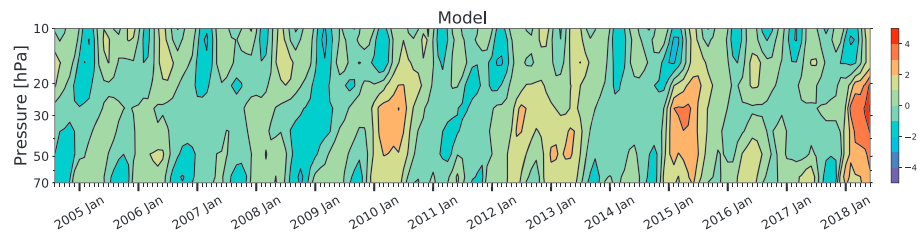The MLS-measured CO data averaged over 15°S to 15°N are shown in Figure 1a. The data have been deseasonalized and normalized to have standard deviation of unity (see Figure S1 in the supporting information for the steps leading from raw data to the final product). A seasonal cycle is estimated by taking the average of data in each month. Then we remove the seasonal cycle from the raw data. Finally, we scale the data by the standard deviation of the deseasonalized data, so that the resulting time series has standard deviation of unity. The CO variability near the tropopause is dominated by the seasonal penetration of air from the troposphere. The major interannual variability in the middle of the stratosphere is QBO, as illustrated by the zonal winds over Singapore (see Figure 1b, derived from raw data in steps shown in Figure S2). The Singapore wind is used as the QBO index in this paper, which is the raw measurement, not the reanalysis data. We have compared the Singapore wind with the zonal wind estimated from NCEP2 reanalysis, and they show consistency.

A climatology of NCEP2 stream function from January 1979 to August 2018 is shown in Figure 2a. The solid contours represent clockwise motions, while dotted represent counterclockwise ones. Air rises in the tropical region, moving toward polar region, and then sinks in the subtropics as part of the Brewer-Dobson circulation (Brewer, 1949; Dobson, 1956). The Brewer-Dobson circulation is primarily responsible for the transport of CO in the middle atmosphere, while K_{yy} and K_{zz} play minor roles (Jiang et al., 2004; Shia et al., 1989).

During different phases of QBO, there is an anomalous motion in the Brewer-Dobson circulation (Plumb & Bell, 1982), which can modulate CO mixing ratio in the stratosphere. To estimate the QBO component of stream function, we apply a principal component analysis (PCA) to the stream function anomalies. Annual cycle and linear trend have been removed from the stream function. In addition, we also apply a lowpass filter to the deseasonalized and detrended stream function anomalies. The lowpass filter is constructed to only keep signals with periods longer than 15 months (Jiang et al., 2004). PCA can decompose the stream function into empirical orthogonal functions (EOFs) and associated principal component (PC) time series. The first leading mode captures 64.1% of the total variance. The spatial pattern of the leading mode is shown in Figure 2b. The power spectrum of PC1 is shown in Figure 2c. PC1 time series and inverted 20-hPa QBO index are plotted in Figure 2d. There is a 28-month signal in the power spectrum of PC1. The correlation coefficient between PC1 and inverted 20-hPa QBO index is 0.78. When the 20-hPa QBO index is in the westerly phase, PC1 is negative, which suggests that the Brewer-Dobson circulation is weakened. When the QBO is in the easterly phase, PC1 is positive, and Brewer-Dobson circulation is strengthened. The change of Brewer-Dobson circulation due to the QBO will modulate CO concentrations at different altitudes.

The second and third modes of the stream function in the PCA are shown Figures S5 and S6, respectively. The second mode is dominated by the QBO-annual-beat with a period of about 20 months (Jiang et al., 2004). The third mode is again dominated by the QBO. For comparison we also plot the first mode in Figure S4. The three modes contribute 64.1%, 21.2%, and 6.6 %, respectively, to the total variance of the stream function, summing up to 91.9% of the total variance.

Figure 3 shows the normalized model-simulated CO mixing ratio. It covers a time period from June 2004 to June 2018. The normalized model CO mixing ratio demonstrates a QBO signal in the stratosphere. We present detailed comparisons between model CO, QBO, and CO data from MLS in Figures 4–6 at 15 hPa. Above this level, the QBO signal in the NCEP2 meridional wind becomes unrealistic because NCEP2 products do not extend beyond 3 hPa. At pressure levels higher than 15 hPa, the QBO signal in CO mixing ratio will have

Figure 4. (a) Time series of normalized model CO (black) and normalized quasi-biennial oscillation (QBO) index (red) at 15 hPa. The normalized QBO index is shifted backward by 7 months. (b) Scatter plot of model CO and QBO index. Time is from 1979 to 2018. It shows a correlation coefficient of $r = 0.795$ between these two quantities. (c and d) Same as (a) and (b) but from 1979 to 2010 with $r = 0.801$. (e and f) Same as (a) and (b) but from 2010 to 2018 with $r = 0.799$.
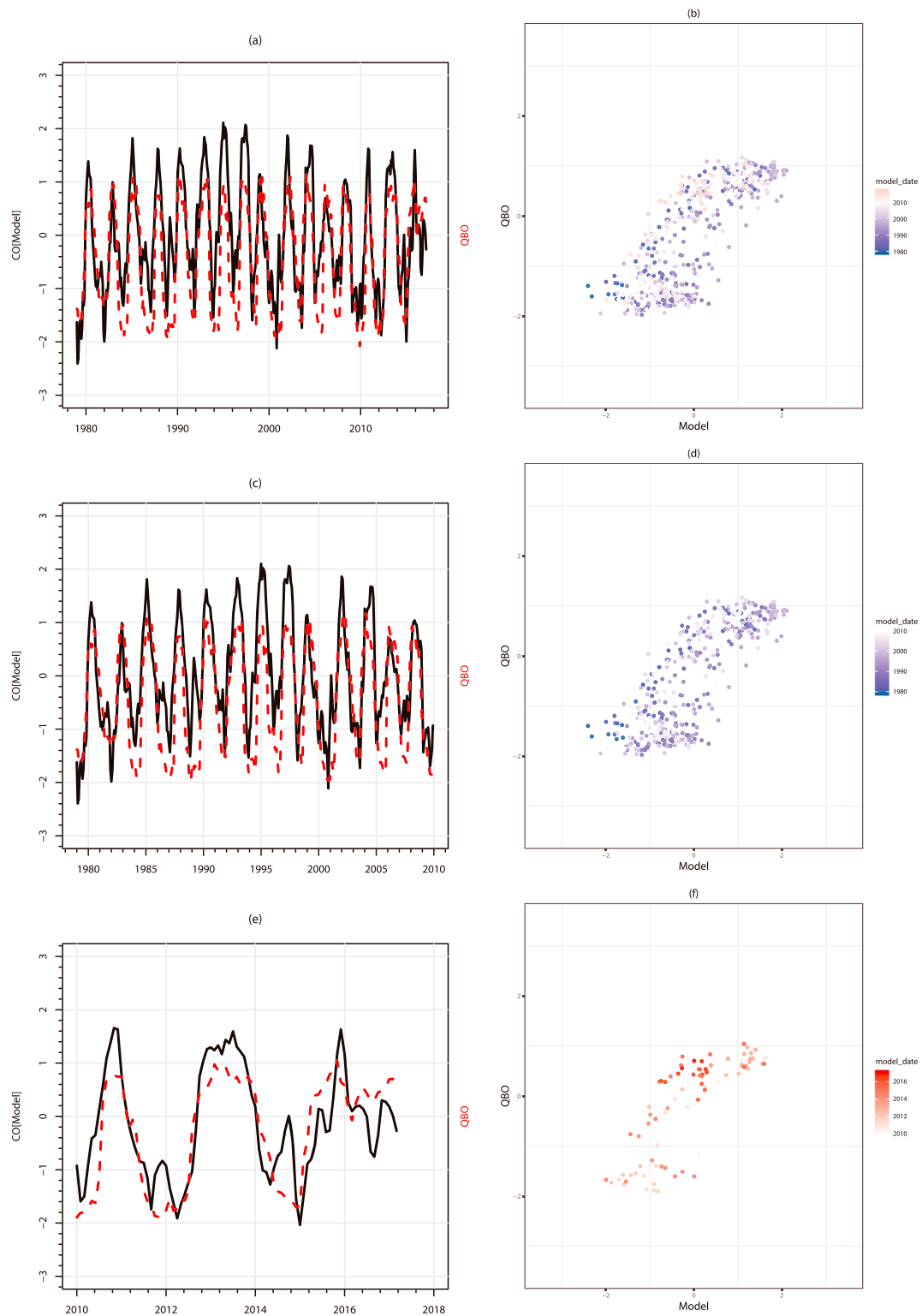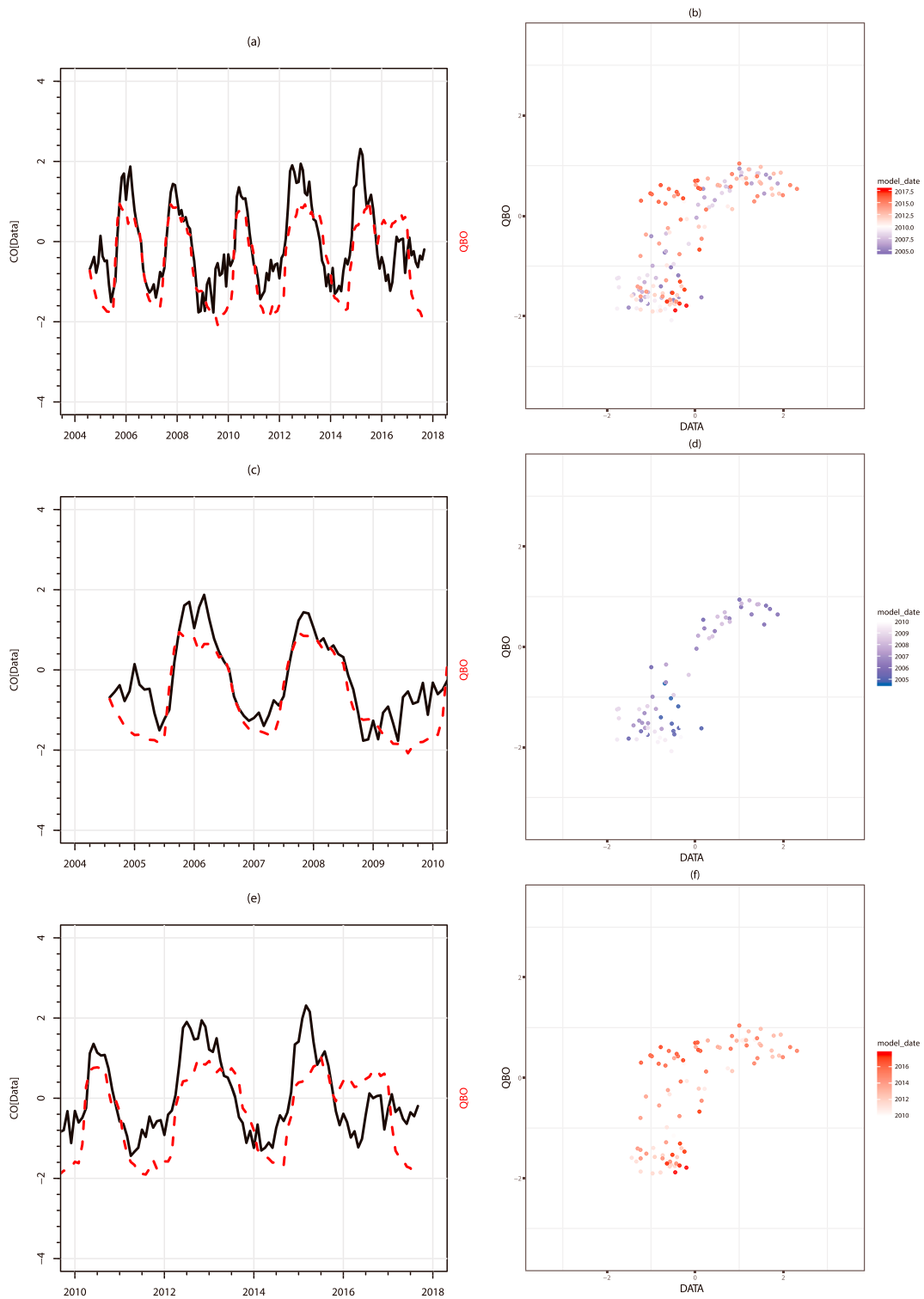
Figure 5. (a) Normalized time series for Microwave Limb Sounder CO (black) and normalized quasi-biennial oscillation (QBO) index (red) at 15 hPa. The normalized QBO index is shifted backward by 11 months. (b) Scatter plot of model CO and QBO index. Time is from 2004 to 2018. It shows a correlation coefficient of $r = 0.765$ between these two quantities. (c and d) Same as (a) and (b) but from 2004 to 2010 with $r = 0.868$. (e and f) Same as (a) and (b) but from 2010 to 2018 with $r = 0.679$.
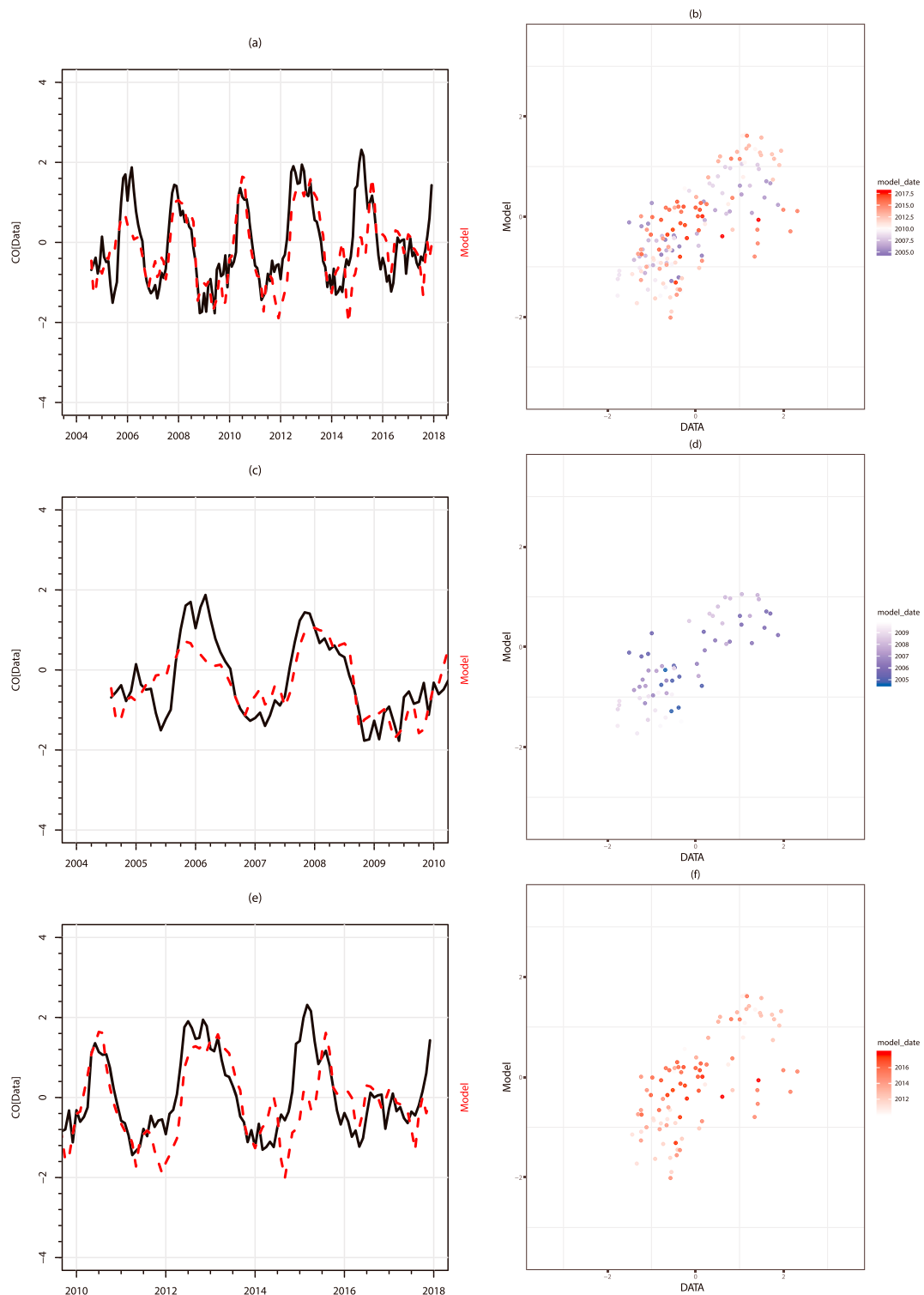
Figure 6. (a) Normalized time series for Microwave Limb Sounder CO (black) and normalized model CO (red) at 15 hPa. The model CO is shifted backward by 4 months. (b) Scatter plot of model CO and Microwave Limb Sounder CO. Time is from 2004 to 2018. It shows a correlation coefficient of $r = 0.720$ between these two quantities. (c and d) Same as (a) and (b) but from 2004 to 2010 with $r = 0.787$. (e and f) Same as (a) and (b) but from 2010 to 2018 with $r = 0.676$.

Table 1
Time Shift and Correlation Between Time Series

	Months shifted backward			Correlation		
	QBO	Model CO	MLS CO	All	Before 2010	After 2010
Figure 4	7	0		0.795	0.801	0.800
Figure 5	11		0	0.765	0.868	0.679
Figure 6		4	0	0.720	0.787	0.676
		(0)[a]	0	0.163	0.349	0.478
Figure S7	11	0		0.685	0.648	0.806
Figure S8	11		0	0.647	0.647	0.647
Figure S9		0	0	0.515	0.384	0.556
		(4)[a]	0	0.316	0.209	0.289

Note. QBO = quasi-biennial oscillation; MLS = Microwave Limb Sounder.
[a]The numbers in parentheses for Figures 6 and S9 indicate hypothetical cases, in which the model CO has been shifted backward by the designated number of months. Only correlations for the hypothetical cases are shown in this table. The time series for these cases are not plotted.

a large interference due to quasi-isentropic mixing with the extratropics. The results for 15 hPa in Figures 4–6 may be compared to those for 20 hPa in Figures S7–S9. The overall correlation between the QBO index and CO mixing ratio is better at 15 hPa than that at 20 hPa, as summarized in Table 1.

Figure 4a shows the QBO signal in the model at 15 hPa from 1979 to 2018. The correlation between CO and the QBO index (shifted backward by 7 months) is 0.795. The scatter plot (Figure 4b) suggests that deviants are mainly from the later years. As shown in Figures 4c–4f, the correlation coefficients between the model simulated CO and QBO index is 0.801 over 1979–2010 and 0.799 over 2010–2018 period. It is clear that more discrepancy arises from the anomalous QBO behavior during the 2015–2016 El Niño years. A phase shift of 7 months arises between CO and the QBO index because the QBO index is based on the zonal wind, whereas the model CO is a mixing ratio. The QBO signal in CO mixing ratio is derived from a combination of the QBO transport discussed earlier and the gradient in CO mixing ratio. The later reflects a balance between chemical production and loss and transport.

Figure 5a shows the QBO signal for CO from MLS, along with the QBO index. The correlation coefficient between MLS CO and QBO (shifted backward by 11 months) is 0.765, which suggests a clear QBO signal in the MLS CO mixing ratio. We notice that the correlation is better before 2010 (Figures 5c and 5d; correlation = 0.868) than after 2010 (Figures 5e and 5f; correlation = 0.679) because of the QBO anomaly during 2015–2016.

Figure 6a shows a comparison of CO obtained from MLS with simulated CO (shifted backward by 4 months). A strong relation is seen between the two time series, as shown in the scatter plot (Figure 6b; correlation = 0.720). We notice that the correlation is slightly higher before 2010 (Figures 6c and 6d; correlation = 0.787) than after (Figures 6e and 6f; correlation = 0.676). We do not have a good reason for the phase shift of 4 months between the model and MLS CO mixing ratios, but we notice four things. (1) The 4-month phase shift is robust by an experiment we carried out in Table 1. We repeated the comparison in Figure 6a, albeit setting the phase shift to 0. In this case, the correlation between the model and MLS CO mixing ratios decreases to 0.163, which is significantly lower than the original value of 0.720. (2) Fifteen hectopascals may be too close to the upper boundary, 3 hPa, above which we have NCEP2 data for deriving a realistic QBO circulation. Indeed, Figure S9a shows the same results as those for Figure 6a, except for 20 hPa, which is farther away from 3 hPa. It has a correlation of 0.515, while the phase shift in this case is 0. (3) To demonstrate the robustness of the aforementioned 0 shift, we shifted the time series for model CO in Figure S9a by 4 months. The resulting correlation is 0.318, which is much lower than the original 0.515. See Table 1 for details. (4) The phase shift of 4 months between the model and MLS CO mixing ratios is consistent with the corresponding shifts of 7 months between the QBO index and model CO, and of 11 months (=4 months + 7 months) between the QBO index and MLS CO.

The results for 15 hPa displayed in Figures 4–6 are compared with those for 20 hPa in Figures S7–S9. The correlation of CO with QBO at 20 hPa is not as high as that at 15 hPa. However, we notice that the years
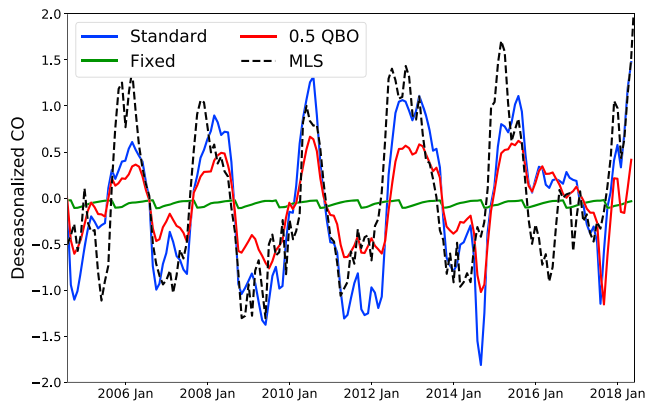
Figure 7. Deseasonalized time series for CO at 15 hPa. Microwave Limb Sounder (MLS) CO is shown as black dashed line. Standard simulation for model CO is shown as blue line. Simulations with no quasi-biennial oscillation (QBO) signal and $0.5 \times$ QBO signal in the stream function are shown as green line and red line, respectively.

with anomalous QBO (after 2010) have better correlation between CO and QBO than that of the years with normal QBO (before 2010).

The QBO signal in the straosphere is the result of a delicate balance between transport and chemistry, as shown in the following sensitivity tests. The EOF and PC analysis of the NCEP2 stream function (see Figure 2) demonstrate the spatial and temporal variation of the QBO signal in the stream function. The deseasonalized CO time series at 15 hPa from this simulation is shown by the green line in Figure 7. In a sensitivity model simulation, we removed the interannual variability of stream function. There is no clear QBO signal in the CO mixing ratio after we removed the interannual variability of the stream function. This suggests that the transport is crucial for generating the QBO signal in the CO mixing ratio. We also conduct another sensitivity test, in which we reduce the QBO component in the stream function by 50%. The result is shown as the red line in Figure 7. As revealed in this simulation (red line), the QBO signal in the CO mixing ratio is reduced compared to the original simulation (blue line).

The primary chemical loss of CO is by the reaction with OH. To study the sensitivity of the QBO signal to chemistry, we reduce the rate coefficient of this reaction by 50%. The results are shown in Figure 8 (green line), where the QBO signal in the reduced loss run is enhanced. When the loss rate is smaller, CO mixing ratio becomes higher. Hence, the QBO-induced transport would introduce a large change in the CO mixing ratio. The opposite happens when the rate coefficient is enhanced by a factor of 2. In the case, the CO mixing ratio is lower, and the QBO signal is reduced (red line).

An interesting question arises whether CH_4 could be an important source of CO in the middle of the stratosphere. The limiting reaction is the slow reaction

$$CH_4 + OH \longrightarrow CH_3 + H_2O \quad k_1 = 2.45 \times 10^{-12} \exp(-1,775/T).$$
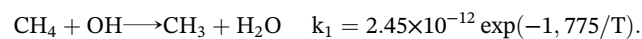
The primary chemical sink is the reaction

$$CO + OH \longrightarrow CO_2 + H \quad k_2 = 1.50 \times 10^{-13},$$

where the rate cofficients are in units of molecules per cubic centimeter per second and T is the ambient temperature in K. It is a good approximation that each molecule of CH_3 eventually produces in a molecule of CO. If the abundance of CO where determined by the chemical equilibrium between these two reactions, we have

$$k_1[CH_4] = k_2[CO]$$

or

$$[CO]/[CH_4] = k_1/k_2 = 16.3\exp(-1,775/T),$$

where [CO] and $[CH_4]$ are the mixing ratios of CO and CH_4, respectively. At stratospheric pressures of 60, 30, and 15 hPa, temperatures (T) are 199, 212, and 223 K, respectively. We estimate [CO] to be 3.5, 6.0, and 8.0 ppbv. These values are of the same order of magnitude as those computed in our model (see Figure S3). Thus, CH_4 is a nontrivial source of CO in the middle stratosphere.
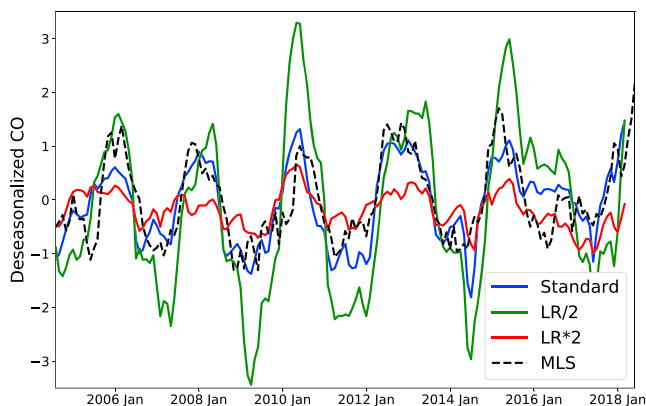

Figure 8. Deseaonalized time series for CO at 15 hPa. Microwave Limb Sounder (MLS) CO is shown as black dashed line. Standard simulation for model CO is shown as blue line. Simulations with reduced chemical rate coefficient (50%) and enhanced chemical rate coefficient (200%) are shown as green line and red line, respectively.

4. Conclusion

The MLS data for CO in the tropical stratosphere clearly demonstrate that QBO drives the dominant variabilities, with high correlation. The 2-D

Caltech/JPL CTM is able to simulate the QBO variability in CO with considerable skill including the anomalous years 2015–2016. The middle atmosphere provides a sensitive indicator for the dynamical activities and their trend in the troposphere (Dunkerton, 2016, 2017; Kawatani & Hamilton, 2013; Newman et al., 2016). We support the statement that "QBO amplitude in the lowermost stratosphere is a consistent projection of global models and represents a subtle, but telling, part of the 'fingerprint' of the expected response of the climate system to anthropogenic climate forcing" (Kawatani & Hamilton, 2013). However, uncertainties remain, especially for solar cycle variabilities in CO (Lee et al., 2018) and HOx chemistry (Li et al., 2017; Wang et al., 2013).

References

Allen, D. R., Stanford, J. L., López-Valverde, M. A., Nakamura, N., Lary, D. J., Douglass, A. R., et al. (1999). Observations of middle atmosphere CO from the UARS ISAMS during the early northern winter 1991/1992. *Journal of the Atmospheric Sciences*, *56*(4), 563–583. https://doi.org/10.1175/1520-0469(1999)056<0563:OOMACF>2.0.CO;2

Allen, D. R., Stanford, J. L., Nakamura, N., López-Valverde, M. A., López-Puertas, M., Taylor, F. W., & Reinedlos, J. J. (2000). Antarctic polar descent and planetary wave activity observed in ISAMS CO from April to July 1992. *Geophysical Research Letters*, *27*(5), 665–668. https://doi.org/10.1029/1999GL010888

Allen, M., Yung, Y. L., & Waters, J. W. (1981). Vertical transport and photochemistry in the terrestrial mesosphere and lower thermosphere (50-120 Km). *Journal of Geophysical Research*, *86*(A5), 3617–3627. https://doi.org/10.1029/JA086iA05p03617

Baldwin, M. P., Gray, L. J., Dunkerton, T. J., Hamilton, K., Haynes, P. H., Randel, W. J., et al. (2001). The quasi-biennial oscillation. *Reviews of Geophysics*, *39*(2), 179–229. https://doi.org/10.1029/1999RG000073

Brewer, A. W. (1949). Evidence for a world circulation provided by the measurements of helium and water vapour distribution in the stratosphere. *Quarterly Journal of the Royal Meteorological Society*, *75*(326), 351–363. https://doi.org/10.1002/qj.49707532603

DeMore, W. B., Howard, C. J., Golden, D. M., Kolb, C. E., Hampson, R. F. & Molina, M. J. (1997). Chemical kinetics and photochemical data for use in stratospheric modeling. JPL Publication, 97-4.

Dobson, G. M. B. (1956). Origin and distribution of the polyatomic molecules in the atmosphere. *Proceedings of the Royal Society of London. Series A. Mathematical and Physical Sciences*, *236*(1205), 187–193. https://doi.org/10.1098/rspa.1956.0127

Dunkerton, T. J. (2016). The quasi-biennial oscillation of 2015–2016: Hiccup or death spiral? *Geophysical Research Letters*, *43*, 10,547–10,552. https://doi.org/10.1002/2016GL070921

Dunkerton, T. J. (2017). Nearly identical cycles of the quasi-biennial oscillation in the equatorial lower stratosphere. *Journal of Geophysical Research: Atmospheres*, *122*, 8467–8493. https://doi.org/10.1002/2017JD026542

Fleming, E. L., Jackman, C. H., Rosenfield, J. E., & Considine, D. B. (2002). Two-dimensional model simulations of the QBO in ozone and tracers in the tropical stratosphere. *Journal of Geophysical Research*, *107*(D23), 4665. https://doi.org/10.1029/2001JD001146

Garcia, R. R., Marsh, D. R., Kinnison, D. E., Boville, B. A., & Sassi, F. (2007). Simulation of secular trends in the middle atmosphere, 1950–2003. *Journal of Geophysical Research*, *112*(D9), D09301. https://doi.org/10.1029/2006JD007485

Gunson, M. R., Farmer, C. B., Norton, R. H., Zander, R., Rinsland, C. P., Shaw, J. H., & Gao, B. –. C. (1990). Measurements of CH_4, N_2O, CO, H_2O, and O_3 in the middle atmosphere by the Atmospheric Trace Molecule Spectroscopy Experiment on Spacelab 3. *Journal of Geophysical Research*, *95*(D9), 13,867–13,882. https://doi.org/10.1029/JD095iD09p13867

Huang, L., Jiang, J. H., Murry, L., Damon, M., Su, H., & Livesey, N. (2016). Evaluation of UTLS carbon monoxide simulations in GMI and GEOS-Chem chemical transport models using Aura MLS observations. *Atmospheric Chemistry and Physics*, *16*(9), 5641–5663. https://doi.org/10.5194/acp-16-5641-2016

Jiang, J. H., Livesey, N. J., Su, H., Neary, L., McConnell, J. C., & Richards, N. A. (2007). Connecting surface emissions, convective uplifting, and long-range transport of carbon monoxide in the upper-troposphere: New observations from the Aura Microwave Limb Sounder. *Geophysical Research Letters*, *34*, L18812. https://doi.org/10.1029/2007GL030638

Jiang, X., Camp, C. D., Shia, R., Noone, D., Walker, C., & Yung, Y. L. (2004). Quasi-biennial oscillation and quasi-biennial oscillation-annual beat in the tropical total column ozone: A two-dimensional model simulation. *Journal of Geophysical Research*, *109*, D16305. https://doi.org/10.1029/2003JD004377

Kane, R. P. (2005). QBO and QTO of the atmospheric trace element carbon monoxide during 1989-2001: An update. *Atmospheric Environment*, *39*(28), 5125–5136. https://doi.org/10.1016/j.atmosenv.2005.05.008

Kawatani, Y., & Hamilton, K. (2013). Weakened stratospheric quasibiennial oscillation driven by increased tropical mean upwelling. *Nature*, *497*(7450), 478–481. https://doi.org/10.1038/nature12140

Kistler, R., Collins, W., Saha, S., White, G., Woollen, J., Kalnay, E., et al. (2001). The NCEP-NCAR 50-year reanalysis: Monthly means CD-ROM and documentation. *Bulletin of American Meteorological Society*, *82*(2), 247–267. https://doi.org/10.1175/1520-0477(2001)082<0247:TNNYRM>2.3.CO;2

Lee, J. N., Wu, D. L., Manney, G. L., Schwartz, M. J., Lambert, A., Livesey, N. J., et al. (2011). Aura microwave limb sounder observations of the polar middle atmosphere: Dynamics and transport of CO and H_2O. *Journal of Geophysical Research*, *116*, D05110. https://doi.org/10.1029/2010JD014608

Lee, J. N., Wu, D. L., & Ruzmaikin, A. (2013). Interannual variations of MLS carbon monoxide induced by solar cycle. *Journal of Atmospheric and Solar-Terrestrial Physics*, *102*, 99–104. https://doi.org/10.1016/j.jastp.2013.05.012

Lee, J. N., Wu, D. L., Ruzmaikin, A., & Fontenla, J. (2018). Solar cycle variations in mesospheric carbon monoxide. *Journal of Atmospheric and Solar-Terrestrial Physics*, *170*, 21–34. https://doi.org/10.1016/j.jastp.2018.02.001

Li, K.-F., Zhang, Q., Wang, S., Sander, S. P., & Yung, Y. L. (2017). Resolving model-observation discrepancy in the mesospheric and stratospheric HOx chemistry. *Earth and Space Science*, *4*, 607–624. https://doi.org/10.1002/2017EA000283

Lindzen, R. S. (1981). Turbulence and stress owing to gravity wave and tidal breakdown. *Journal of Geophysical Research*, *86*(C10), 9707–9714. https://doi.org/10.1029/JC086iC10p09707

Livesey, N. J., Filipiak, M. J., Froidevaux, L., Read, W. G., Lambert, A., Santee, M. L., et al. (2008). Validation of Aura Microwave Limb Sounder O-3 and CO observations in the upper troposphere and lower stratosphere. *Journal of Geophysical Research*, *113*, D15S02. https://doi.org/10.1029/2007JD008805

Livesey, N. J., Read, W. G., Wagner, P. A., Froidevaux, L., Lambert, A., Manney, G. L., et al. (2015). *EOS MLS Version 4.2x Level 2 data quality and description document, EOS MLS data documentation*. Pasadena, CA: Jet Propulsion Laboratory, California Institute of Technology.

Minschwaner, K., Manney, G. L., Livesey, N. J., Pumphrey, H. C., Pickett, H. M., Froidevaux, L., et al. (2010). The photochemistry of carbon monoxide in the stratosphere and mesosphere evaluated from observations by the Microwave Limb Sounder on the Aura satellite. *Journal of Geophysical Research*, *115*, D13303. https://doi.org/10.1029/2009JD012654

Morgan, C. G., Allen, M., Liang, M. C., Shia, R. L., Blake, G. A., & Yung, Y. L. (2004). Isotopic fractionation of nitrous oxide in the stratosphere: Comparison between model and observations. *Journal of Geophysical Research*, *109*, D04305. https://doi.org/10.1029/2003JD003402

Newman, P. A., Coy, L., Pawson, S., & Lait, L. R. (2016). The anomalous change in the QBO in 2015–2016. *Geophysical Research Letters*, *43*, 8791–8797. https://doi.org/10.1002/2016GL070373

Plumb, R. A., & Bell, R. C. (1982). A model of the quasi-biennial oscillation on an equatorial beta-plane. *Quarterly Journal of the Royal Meteorological Society*, *108*(456), 335–352. https://doi.org/10.1002/qj.49710845604

Ruzmaikin, A., Lee, J. N., & Wu, D. L. (2014). Patterns of carbon monoxide in the middle atmosphere and effects of solar variability. *Advances in Space Research*, *54*(3), 320–326. https://doi.org/10.1016/j.asr.2013.06.033

Schoeberl, M. R., Duncan, B. N., Douglass, A. R., Waters, J., Livesey, N., Read, W., & Filipiak, M. (2006). The carbon monoxide tape recorder. *Geophysical Research Letters*, *33*, L12811. https://doi.org/10.1029/2006GL026178

Shia, R. L., Yung, Y. L., Allen, M., Zurek, R. W., & Crisp, D. (1989). Sensitivity study of advection and diffusion coefficients in a 2-dimensional stratospheric model using excess ^{14}C data. *Journal of Geophysical Research*, *94*(D15), 18,467–18,484. https://doi.org/10.1029/JD094iD15p18467

Sitnov, S. A. (2008). Analysis of the quasi-biennial variability of carbon monoxide total column. *Atmospheric and Oceanic Physics*, *44*(4), 459–466. https://doi.org/10.1134/S0001433808040063

Solomon, S., Garcia, R. R., Olivero, J. J., Bevilacqua, R. M., Schwartz, P. R., Clancy, R. T., & Muhleman, D. O. (1985). Photochemistry and transport of carbon monoxide in the middle atmosphere. *Journal of the Atmospheric Sciences*, *42*(10), 1072–1083. https://doi.org/10.1175/1520-0469(1985)042<1072:PATOCM>2.0.CO;2

Summers, M. E., Siskind, D. E., Bacmeister, J. T., Conway, R. R., Zasadil, S. E., & Strobel, D. F. (1997). Seasonal variation of middle atmospheric CH_4 and H_2O with a new chemical-dynamical model. *Journal of Geophysical Research*, *102*(D3), 3503–3526. https://doi.org/10.1029/96JD02971

Wang, S., Li, K. F., Pongetti, T. J., Sander, S. P., Yung, Y. L., Liang, M. C., et al. (2013). Midlatitude atmospheric OH response to the most recent 11-y solar cycle. *Proceedings of the National Academy of Sciences of the United States of America*, *110*(6), 2023–2028. https://doi.org/10.1073/pnas.1117790110

Waters, J. W., Froidevaux, L., Harwood, R. S., Jarnot, R. F., Pickett, H. M., Read, W. G., et al. (2006). The Earth Observing System Microwave Limb Sounder (EOS MLS) on the Aura satellite. *IEEE Transactions on Geoscience and Remote Sensing*, *44*(5), 1075–1092. https://doi.org/10.1109/TGRS.2006.873771